

Physical and Electrochemical Properties of LiFePO₄/C Nanofibers Synthesized by Electrospinning

Huei-Yu Lin¹, Shun-Mao Yeh², Jenn-Shing Chen^{1,*}

¹Department of Applied Chemistry, National University of Kaohsiung, Kaohsiung City, Taiwan 811, R.O.C.

²Department of Electrical Engineering, National University of Kaohsiung, Kaohsiung City, Taiwan 811, R.O.C.

*E-mail: jschen@nuk.edu.tw

Received: 5 August 2014 / Accepted: 11 September 2014 / Published: 29 September 2014

One dimensional LiFePO₄/C composite nanofibers were prepared by electrospinning. Polyacrylonitrile (PAN) is used as both the electrospinning media and as the carbon source. LiFePO₄ precursors and PAN were dissolved in *N,N*-dimethylformamide (DMF) before electrospinning. LiFePO₄ precursors/PAN fibers were heat treated, transforming the LiFePO₄ precursors into the olivine structure. Using this method, well-crystallized LiFePO₄/C composite nanofibers were synthesized. The materials were characterized using X-ray diffraction (XRD), scanning electron microscopy (SEM), transmission electron microscopy (TEM), BET surface area, cyclic voltammetry (CV), electrochemical impedance spectroscopy (EIS) and charge-discharge tests. The characterization data reveal that the prepared LiFePO₄/C composite nanofibers with uniformly dispersed carbon particles on the surface. The uniformly dispersed particles furnish the products with very large surface-to-volume ratios with good electronic characteristics. The electrochemical performance of LiFePO₄/C composite nanofibers is markedly improved compared to composites obtained by classical co-precipitation methods. It is found that the LiFePO₄/C composite nanofibers exhibit a higher discharge capacity of 162 mAh g⁻¹ at 0.1C rate.

Keywords: Lithium iron phosphate, Electrospinning, Lithium-ion batteries, Cathode materials

1. INTRODUCTION

Energy storage devices with high energy and power are being developed for use as power source sources for electric vehicles (EV) and hybrid electric vehicles (HEV)[1-5].

Among the various alternative cathode materials, the olivine-structured lithium ion phosphate (LiFePO₄) has attracted much interest owing to its high theoretical capacity (170 mAh), acceptable

operating voltage (3.4 V vs. Li/Li⁺), cycling stability, thermal safety, low cost and environmental friendliness [2-7]. Despite these favorable characteristics, their widespread use is hampered by poor rate performance. The features responsible for the poor rate capability are thought to be its intrinsically poor electronic conductivity (of the order of 10⁻⁹ Scm⁻¹) and the sluggish Li⁺ diffusion that occurs across the LiFePO₄/FePO₄ interface [4, 8-10].

In order to overcome these problems, several strategies have been followed over the years such as optimized synthesis procedures [2, 3, 11-14], particle-size minimization [9, 15-18], carbon nanocoating [15, 19-23], metal powder addition [22, 24], doping with alien cations [2, 4, 25, 26] and the carbothermal formation of the surface conducting phase [17, 22, 23, 27]. It has been well demonstrated that the electrochemical properties of LiFePO₄ could be improved by the incorporation of conductive carbon into active material powders to form carbon-coated LiFePO₄ (LiFePO₄/C) composites [6, 20, 22, 28]. The behavior of these LiFePO₄/C composites is related to the phase purity of the active material, particle sizes, structure of the carbon additive, the carbon content, the form of the carbon contact, and the mixing and sintering recipe. Although there have been many studies regarding LiFePO₄/C and polycrystalline and nanocrystalline materials, few studies have examined the synthesis of LiFePO₄/C nanofibers [9, 29]. In this study, we concentrated on fabricating nanostructured LiFePO₄/C in the form of fibers using a sol-gel method in combination with an electrospinning technique.

The electrospinning technique is a well-know method and was successfully applied to many polymer systems to prepare nano-fibers and nanostructured materials with high specific surface area [9, 29-32]. Hosono et al. [33] reported that a composite nanowire of LiFePO₄/C could be prepared by an electrospinning method using a polymer solution that included Li, Fe, and P sources. Moreover, many authors [9, 29, 34-36] have reported that the electrospinning method is suitable for the synthesis of the LiFePO₄/C composite nanofibers, which have the morphology of one-dimensional LiFePO₄ nanostructures causing a shorter Li⁺ diffusion path. The concentration of polymer-gel solution plays a role in maintaining the fiber-structure in the electrospinning process and the polymer functions as the spinning template and the carbon source. However, the majority of recent work used lower concentrations of LiFePO₄ precursors and higher polymer concentrations for the electrospinning process. This is done in order to obtain excellent fiber-forming ability and chemical stability for the formation of LiFePO₄/C composite nanofibers, causing the residual pyrolyzed carbon from the polymer to be very high (36.6 ~ 20%) resulted in less active materials of LiFePO₄ in the composite nanofibers [33, 35, 36]. Therefore, the goal of this work is to reduce the residual carbon for the preparation of LiFePO₄/C nanofibers via a combination of electrospinning and sol-gel methods. Higher concentrations of LiFePO₄ precursors in the polymer-gel solution were applied to obtain LiFePO₄/C nanofibers of defined size and geometry by controlling the electrospinning parameters. The physicochemical properties and electrochemical behavior of the samples were characterized.

2. EXPERIMENTAL

LiFePO₄ and its carbon composites were prepared using a combination of electrospinning and sol-gel methods. Sol-gel solutions were prepared by dissolving Fe(NO₃)₃·9H₂O (Aldrich, 99%),

LiNO_3 (Aldrich, 99%) and H_3PO_4 (Riedel-deHaën, 85%) in Dimethylformamide (DMF, Aldrich, 99%) at 1:1:1 Li:Fe:P molar ratio, then polyacrylonitrile (PAN, Aldrich, $M_w = 15000$) was added into the above solution under stirring for 2 h. The concentration of PAN dissolved in DMF plays the role of the increasing the spinnability of the solution and the carbon content in the resultant LiFePO_4/C composite nanofibers. The concentrations of LiFePO_4 precursor, PAN and DMF in the spinning solution were 13, 3 and 84 wt%, respectively. The resultant precursor was poured into a syringe with a stainless-steel needle and a positive terminal was connected to the syringe needle tip while an aluminum foil covered a rotating collector worked as counter electrode. A direct-current electric field of 12 kV was applied to the solution through the needle tip and the solution feed rate was 0.15 mLh^{-1} . The distance between the needle tip and collector (aluminum foil) was $\sim 15 \text{ cm}$.

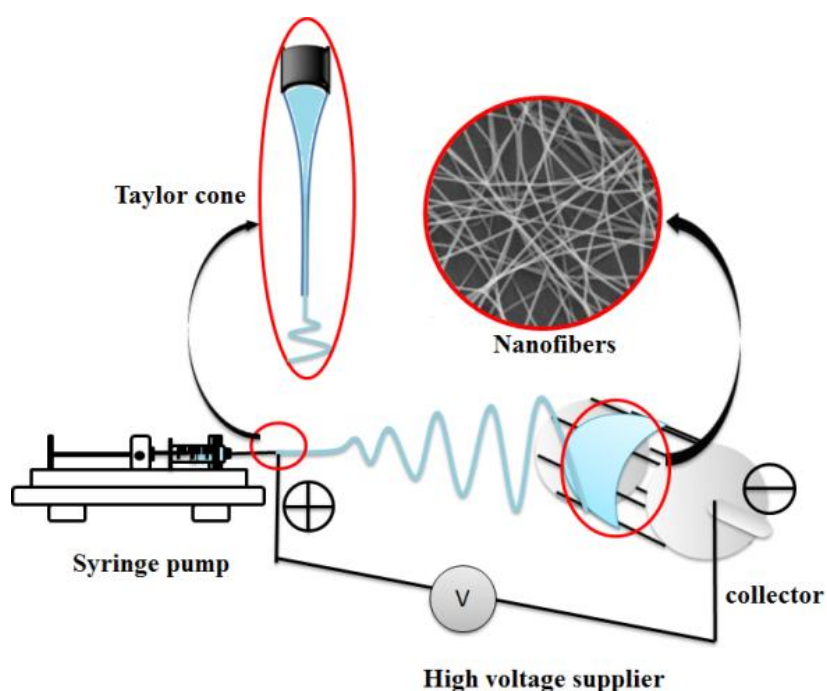


Figure 1. Schematic of the electrospinning setup.

Electrospinning experiments were performed at room temperature with a relative air humidity of 30–40%. Fig. 1 displays a schematic illustration of the electrospinning setup. To obtain LiFePO_4/C composite nanofibers, the as-spun precursor nanofibers were carried out using a two-step heat treatment. First, the precursor nanofibers were stabilized in air environment at $300 \text{ }^\circ\text{C}$ for 5 h with a heating rate of $3 \text{ }^\circ\text{Cmin}^{-1}$ and then calcinated at $800 \text{ }^\circ\text{C}$ for 12 h under reducing atmosphere ($\text{Ar}/\text{H}_2 = 95/5$) with a heating rate of $3 \text{ }^\circ\text{Cmin}^{-1}$ to yield LiFePO_4/C composite nanofibers.

A Rigaku-D/MaX-2550 diffractometer with $\text{Cu K}\alpha$ radiation ($\lambda = 1.54 \text{ \AA}$) was used to obtain X-ray diffraction (XRD) patterns for the samples. The morphology of the sample was observed using a scanning electron microscope (SEM, Hitachi S-4300) and transmission electron microscope (TEM, JEOL JEM-2010). An integrated Raman microscope system, JOBIN-YVON T64000, was used to analyze the structure and composition of the individual particles in LiFePO_4 . Thermogravimetry (TG)

and differential scanning calorimetry (DSC) apparatus (SETARAM) were used for the thermal analysis. The Brunauer-Emmett-Teller (BET) method was used to measure the specific surface area of the powders (ASAP2020). The residual carbon content of the powders was determined by means of an automatic elemental analyzer (Elementar vario, EL III).

For electrochemical evaluation, the composite electrodes were prepared by wet coating, and were made from as-prepared LiFePO_4/C with acetylene black, SFG-6 synthetic flake graphite (Timcal Ltd.), and poly(vinylidene difluoride) (PVDF) binder (MKB-212C, Elf Atochem) in a weight ratio of 80:5:5:10. The LiFePO_4/C active materials, acetylene black and SFG-6 were first added to a solution of PVDF in *N*-methyl-2-pyrrolidone (NMP, Riedel-deHaen). To make a slurry with an appropriate viscosity, the mixture was stirred for 20 minutes at room temperature using a magnetic stir bar, and then for 5 minutes by using a turbine at 2000 rpm. The resulting slurry was coated onto a piece of aluminum foil and dried at 120°C for 40 min. The coating had a thickness of $\sim 100\ \mu\text{m}$ with an active material mass loading of $8 \pm 1\ \text{mg cm}^{-2}$. The quantity of active materials on the electrodes was kept constant.

Electrodes were dried overnight at 100°C under vacuum before being transferred into an argon-filled glove box for cell assembly. For CV experiments, electrodes were placed in an open glass bottle cell with a $1\ \text{cm}^2$ square LiFePO_4/C cathode electrode and lithium foil as the counter and reference electrodes. Coin cells of 2032 size were assembled using lithium metal as a counter electrode. A solution of 1 M LiPF_6 in a mixed solvent of 1:1 (by volume) of ethylene carbonate/dimethyl carbonate (EC/DMC) was used as the electrolyte in all cells. The CV experiments were carried out using a CHI 704A potentiostat using a scan rate of $0.1\ \text{mVs}^{-1}$. Coin cells were cycled galvanostatically with a BAT-750B (Acu Tech System) at a constant current of 0.5C with a voltage region of 2.5–4.2 V vs Li/Li^+ at room temperature; here, 1C equals $170\ \text{mA g}^{-1}$. The current density was calculated based on the mass of LiFePO_4/C in the electrode.

3. RESULTS AND DISCUSSION

TGA/DSC curves (Fig.2) of the PAN and as-spun LiFePO_4 precursor/PAN nanofibers (ASL-PAN) were measured in Ar between 25 and 800°C to investigate the decomposition temperature of the PAN and LiFePO_4 precursors. As can be seen in Fig. 2, PAN produced one exothermic peak at $\sim 311^\circ\text{C}$ with no appreciable weight-loss above 500°C . Moreover, we can observe the weight loss for the ASL-PAN as a function of temperature. It was observed that the fibers lost $\sim 22\%$ of their weight between room temperature and 180°C , and 12% when heated between 180 and 310°C , and finally 13% when heated between 310 – 500°C . Above 500°C , there is no evident weight loss. The first weight loss below 180°C , with one broad endothermic peak at $\sim 137^\circ\text{C}$, is likely due to the loss of water vapor and trapped organic solvent (DMF)[37]. The latter two weight losses are assigned to the burn of PAN and metal salts and to the crystallization of the LiFePO_4 crystal. Two obvious exothermic peaks at ~ 219 and 317°C result from the decomposition of nitrate salts and PAN, respectively[38, 39]. Moreover, as shown in the magnified region of Fig.2, the DSC curve of the ASL-PAN exhibits a small exothermic

peak at 479°C that is related to the transformation of LiFePO_4 compound from an amorphous to a crystalline phase [40].

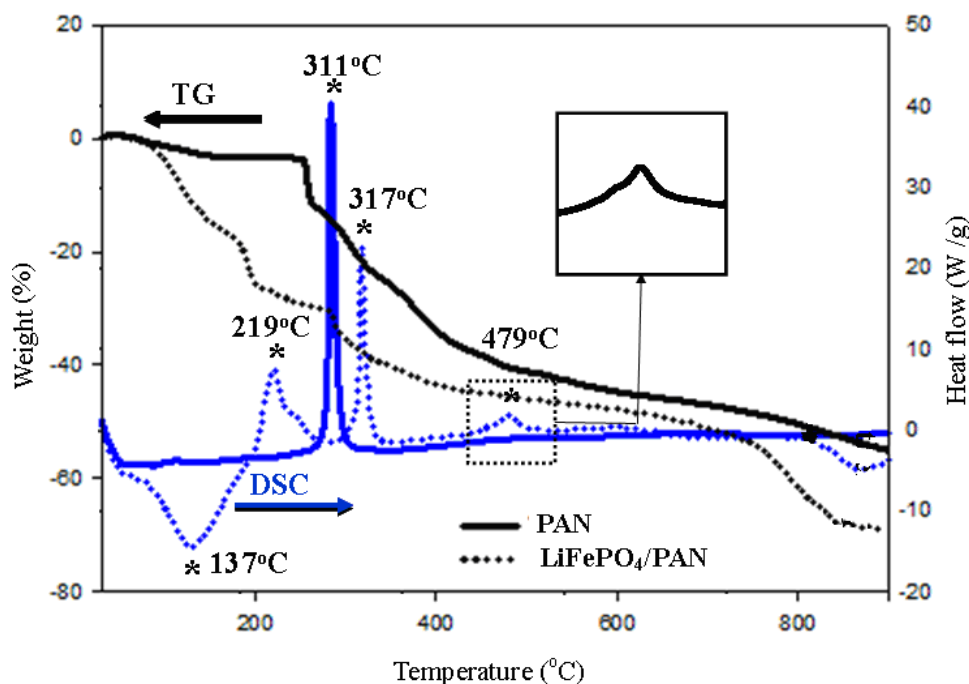


Figure 2. TGA/DSC curves of PAN and as-spun LiFePO_4 precursor/PAN nanofibers (ASL-PAN) before calcination.

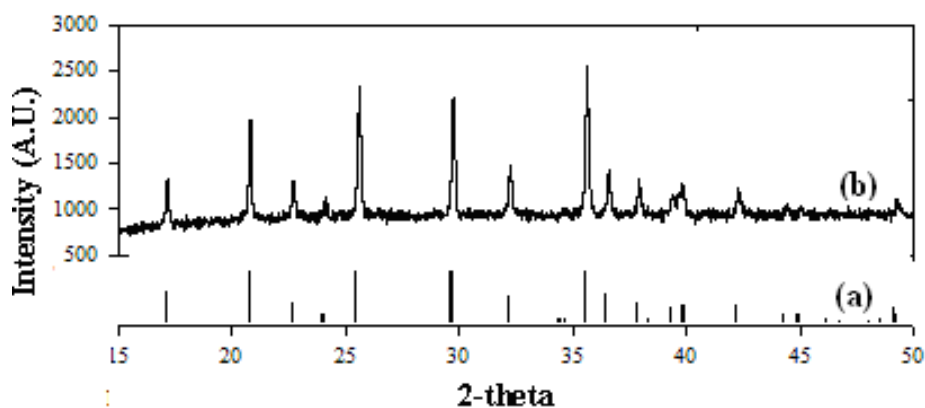


Figure 3. XRD patterns for (a) theoretical pattern, (b) LiFePO_4/C composite nanofibers.

All prepared LiFePO_4/C powders were deep black in color, in contrast to the gray color of pure LiFePO_4 powders. Fig. 3 shows the XRD patterns of the prepared LiFePO_4/C composite nanofibers. All peaks can be identified as a pure and well-crystallized LiFePO_4 phase with an ordered olivine structure indexed to the orthorhombic $Pnmb$ space group. Moreover, no peaks but reflections in the diffractograms of carbon were found in the final product, indicating that carbon generated in the final product by the pyrolysis of PAN is amorphous.

The morphology of the as-spun LiFePO_4 precursor/PAN nanofibers (ASL-PAN) and LiFePO_4/C composite nanofibers were observed using SEM, as shown in Fig. 4. Fig. 4a-b shows the ASL-PAN before calcination. The general appearance of the ASL-PAN displays a fibrous morphology with smooth surface and uniform diameter of ~ 250 nm.

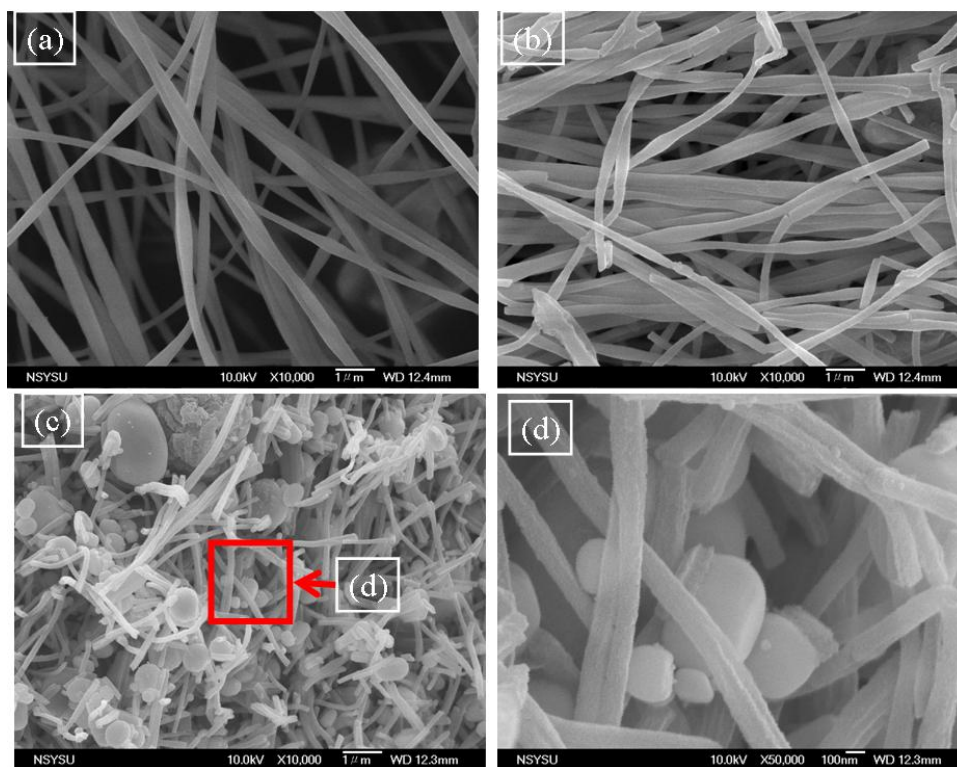


Figure 4. SEM images (a) as-spun LiFePO_4 precursor/PAN nanofibers (ASL-PAN), (b) ASL-PAN after 300°C heat treatment, (c) LiFePO_4/C composite nanofibers after calcination at 800°C , and (d) high magnification of the region marked with a square in (c).

Clearly, our study indicates that the sol-gel solution has excellent spinnability at higher salt concentrations (above 80 wt% in total weight of PAN and salts). After 300°C heat-treatment, the ASL-PAN maintains nanofibrous morphology (Fig 4b) but has a slight decreased diameter with the presence of broken fibers. Fig. 4c-d displays the SEM image of the LiFePO_4/C composite nanofibers after calcination at 800°C . From these images, the nanofiber structure is maintained but the diameter (~ 200 nm) decreased likely due to the decomposition of PAN and inorganic salts. However, higher temperatures (800°C) leads to larger particle sizes, and in this case the fibrous morphology of the sample is slightly destroyed, which results in the production of a few agglomerates and the appearance of some spherical particles in the fibers.

The pore structure of the LiFePO_4/C composite nanofibers was determined by nitrogen adsorption-desorption isothermal measurements. As shown in Fig. 5, the adsorption isothermal curve of the LiFePO_4/C composite nanofibers have a well-defined step as the typical IV classification with a H_1 -type hysteric loop in the p/p_0 range of 0.50 – 1.0, indicating mesoporous material character. These

findings suggest that the LiFePO_4/C composite sample does not contain framework-confined pores but is rather made up of individual nanofibers.

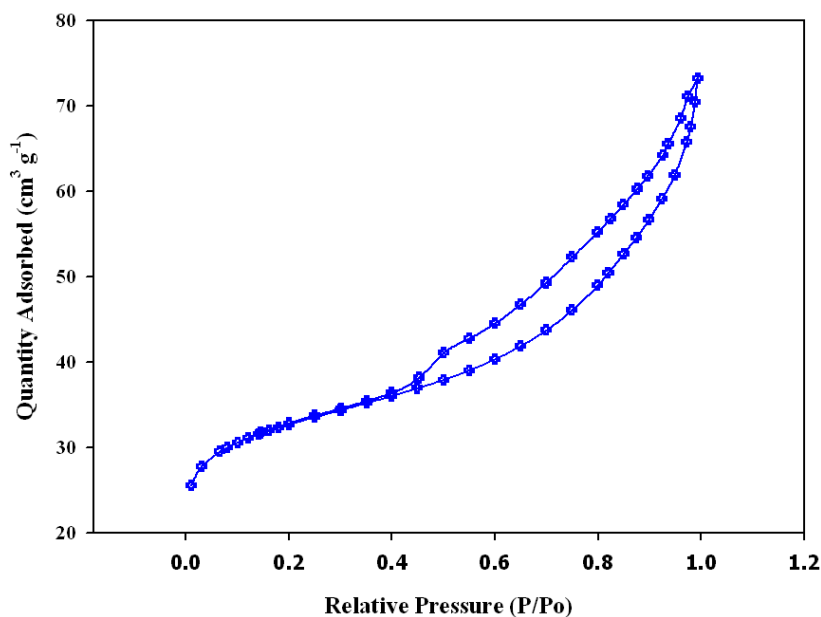


Figure 5. Nitrogen sorption isotherm of the LiFePO_4/C composite nanofibers.

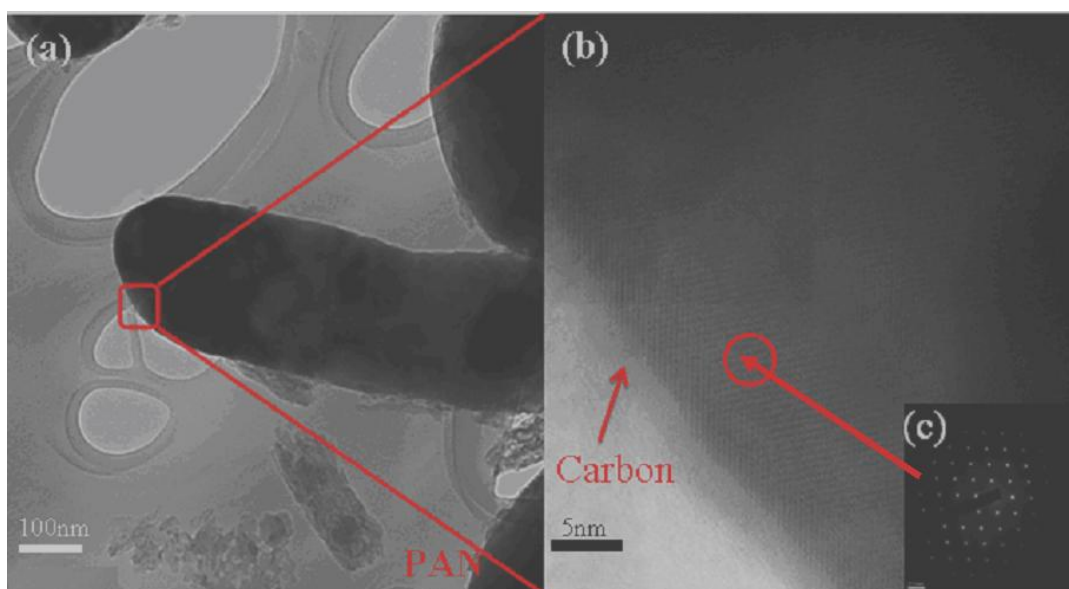


Figure 6. TEM images (a) LiFePO_4/C composite nanofibers, (b) high magnification image of the region of the marked with a square in (a), and (c) lattice image of the region marked with a circle in (b).

This is in agreement with the results from the SEM images. Moreover, the measured BET surface area of LiFePO_4/C composite nanofibers is $111.9 \text{ m}^2 \text{ g}^{-1}$, which is larger than other LiFePO_4/C composite nanofibers prepared from other examples in the literature [29] or our previous LiFePO_4/C

composites prepared using the microemulsion method [12, 13]. Generally, a larger surface area is important for enhancing the electrochemical properties of LiFePO_4 materials [41].

The microstructure of the LiFePO_4/C composite nanofibers was investigated using TEM and corresponding selected-area electron diffraction (SAED). Fig. 6a is a low-magnification image of the LiFePO_4/C composite nanofibers. Fig. 6b shows the magnified region of the marked area in a. The TEM image further testifies the good fibrous morphology and the fiber consists of many crystalline LiFePO_4 grains. The diameter of the fiber in the image is 200 nm, which is also consistent with the SEM results. In addition, the surface of the composite fiber is coated by a layer of carbon species with a thickness of ~ 3 nm and the corresponding SAED of the insert indicates the single-crystal structure of an individual LiFePO_4 grain as shown in Fig. 6b, c.

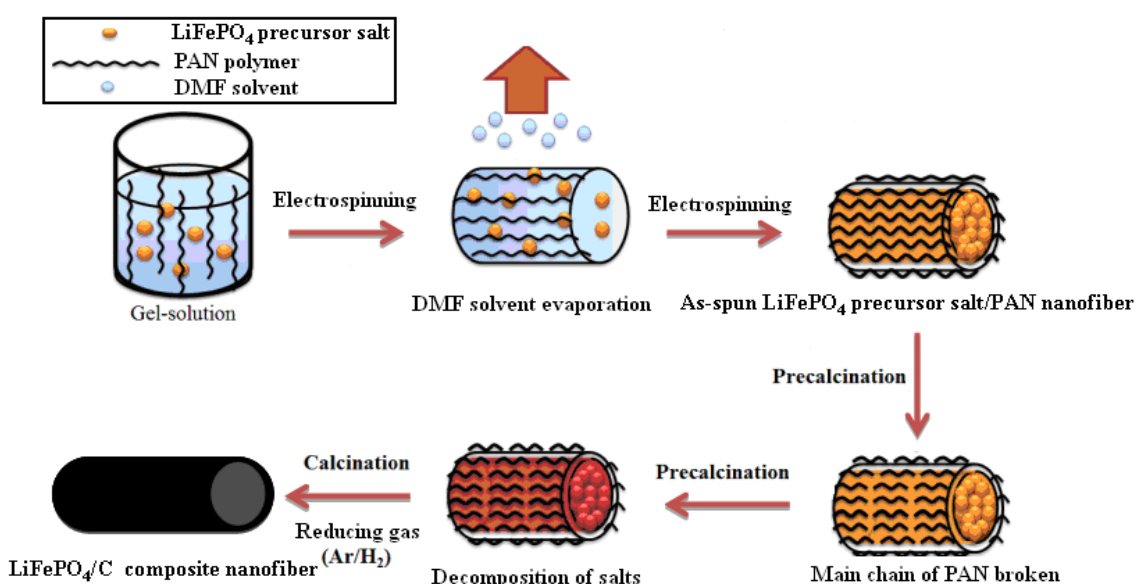


Figure 7. Schematic illustration for the formation of the LiFePO_4/C composite nanofiber.

From the above analytical results, a possible formation mechanism of the LiFePO_4/C composite nanofiber is proposed and is shown in Fig.7. A sol-gel solution appropriate for the electrospinning was prepared by dissolving LiFePO_4 precursor salts and PAN in DMF. Next, the DMF solvent was evaporated in the process of the electrospinning and the as-spun LiFePO_4 precursor salt/PAN nanofiber was obtained. Next, the as-spun nanofibers were carried out two step heat treatment including 300°C precalcination in air followed by 800°C calcination under reducing atmosphere ($\text{Ar}/\text{H}_2 = 95/5$). During precalcination, PAN polymers were oxidized to break their main chains and the inorganic salts were decomposed to produce amorphous LiFePO_4 . Finally, when calcinated at 800°C , a synchronous process of LiFePO_4 crystallization and decomposition of the broken PAN into residual carbon occurs like an in situ synthesis of LiFePO_4/C composite and the residual carbon homogeneously coats on the surface of the LiFePO_4 crystallite nanofiber. For the further exploration of the mechanism, the intermediate products need to be analysed during the formation of the LiFePO_4/C composite nanofiber. Obviously, the PAN in the system plays an important role for an electrospinning template to provide

the spinnability solutions and a highly active carbon source to increase the conductivity of the LiFePO_4 . The measured residual carbon content of LiFePO_4/C composite nanofibers is ~ 15 wt%, which is lower than other LiFePO_4/C composite nanofibers (36.6 \sim 20%) prepared from other literatures [33, 35, 36].

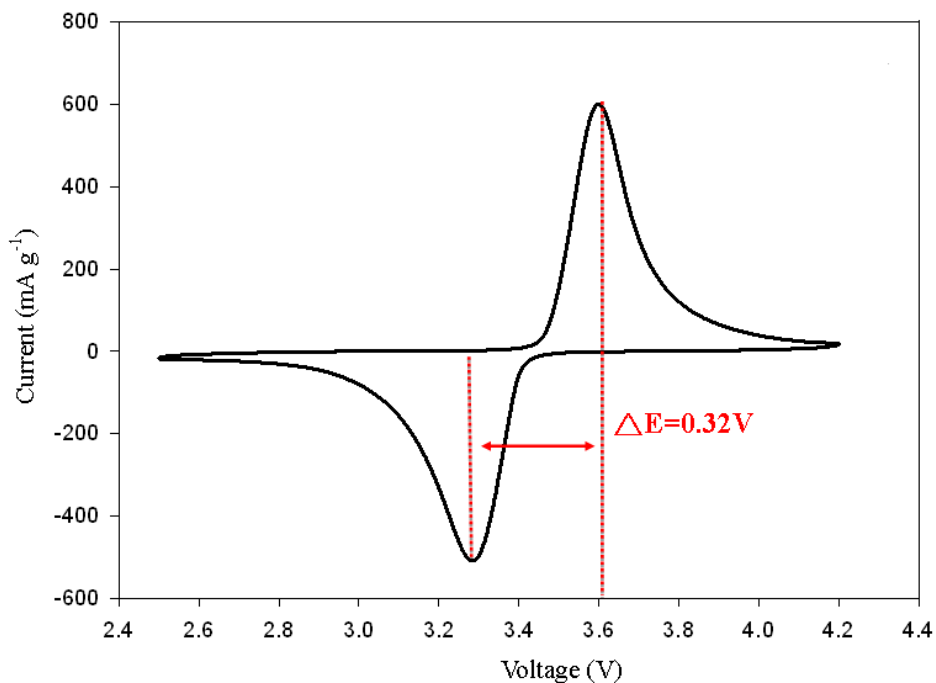


Figure 8. Cyclic voltammogram of the third cycle for the LiFePO_4/C composite nanofibers.

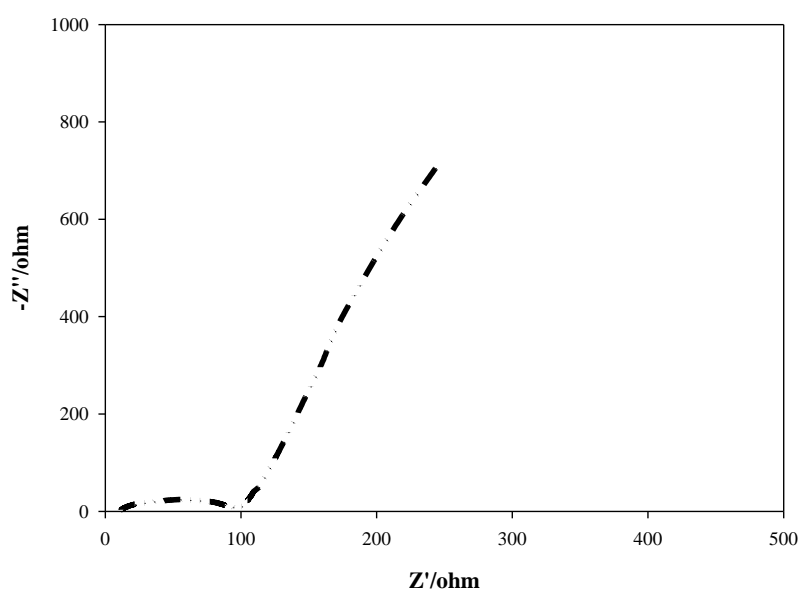


Figure 9. AC impedance spectroscopy of LiFePO_4/C composite nanofibers.

The CV plot of LiFePO₄/C composite nanofibers cycled between 2.5 and 4.2 V with 0.1 mV s⁻¹ and 1 M LiPF₆ + EC/DMC (1:1) electrolyte are shown in Fig. 8. The CV curve exhibited two peaks located at 3.6 V in the anodic sweep and 3.3 V in the cathodic sweep, consistent with a two-phase redox reaction at ~ 3.5 V vs. Li/Li⁺. No other peaks were observed, indicating the absence of electroactive iron impurities. According to the estimation of the CV curve, the sample has a coulombic efficiency of 99%. Electrochemical impedance spectroscopy (EIS) was measured using coin cells in the fully charge state. Fig. 9 shows the typical Nyquist plot of the LiFePO₄/C composite nanofibers. The plot has an intercept at high frequency, followed by a semicircular plot in the medium-to-high frequency region and a sloping line in the low frequency region. The intercept at the Z' axis in the high frequency region corresponds to the ohmic resistance (R_e) of the electrolyte and the electrical contact. The semicircular plot in the medium frequency range can be attributed to the charge transfer resistance (R_{ct}) of the electrochemical reaction and the sloping line in the low frequency region represents the diffusion of lithium ions into the bulk of the cathode material, namely the Warburg impedance[25]. As indicated in Fig. 9, the R_{ct} value for the LiFePO₄/C composite nanofibers is 99 Ω.

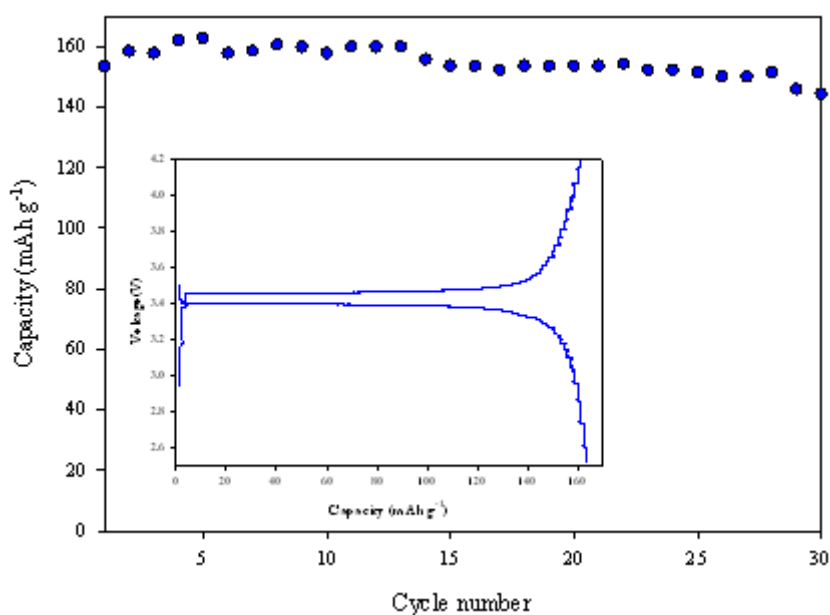


Figure 10. The capacity retention of the LiFePO₄/C composite nanofibers cycled at 0.1C rate between 2.5 and 4.2 V. The insert is the 5th charge/discharge curves.

Fig. 10 shows a plot of capacity versus cycle number for the cell composed of LiFePO₄/C composite nanofibers. The cell displayed stable cycle performance upon 30 repeated cycles. The insert in Fig. 10 shows the charge-discharge voltage profiles of the LiFePO₄/C composite nanofibers at 0.1 C rate between 2.5 and 4.2 V during the 5th cycle. The cell exhibits a charge-discharge curve plateau over a wide voltage range at approximately 3.4 V (vs. Li/Li⁺), implying that a two-phase Fe³⁺/Fe²⁺ redox reaction proceeds via a first-order transition between FePO₄ and LiFePO₄. The small voltage difference between the charge-discharge plateaus of FePO₄ and LiFePO₄ indicates good kinetics. The cell delivers the discharge capacity of 162 mAhg⁻¹ in the 5th cycle which is ~ 95% of the theoretical

capacity (170 mAhg^{-1}). The coulombic efficiency of all samples is approximate 99% which is in good agreement with the CV measurements. Cycle stabilities of the cell with various discharge current rates are presented in Fig. 11. At a rate of 1C, a reversible capacity of 139 mAhg^{-1} can be achieved, which is $\sim 86\%$ of the initial capacity at 0.1C rate.

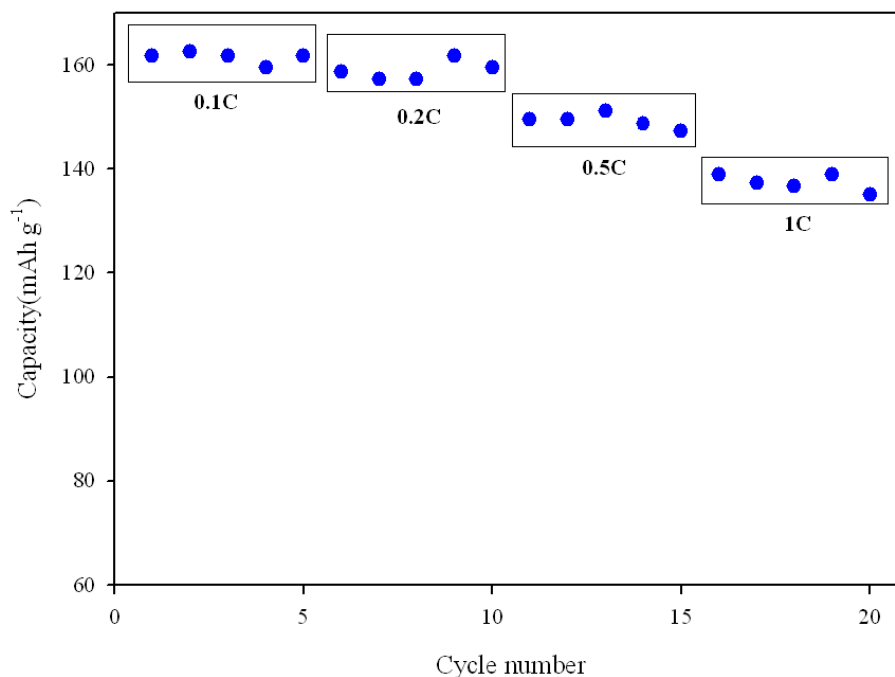


Figure 11. Cycle stability of the LiFePO_4/C composite nanofibers with various discharge current rates.

This retention of LiFePO_4/C capacity shows that the LiFePO_4/C possesses an excellent rate capability and good cycle life. As expected, the excellent electrochemical performance of the LiFePO_4/C composite nanofibers can be attributed to their smaller particle sizes, larger specific surface areas, and highly uniform carbon distribution on the surface of the nanofibers.

4. CONCLUSION

One-dimensional LiFePO_4/C composite nanofibers with lower carbon content have been synthesized using a combination of electrospinning and sol-gel methods. The measured residual carbon of LiFePO_4/C composite nanofibers was $\sim 15 \text{ wt}\%$. The average diameter and BET surface area of LiFePO_4/C composite nanofibers was 200 nm and $111.9 \text{ m}^2\text{g}^{-1}$, respectively. It was found that the LiFePO_4/C composite nanofibers exhibit a higher discharge capacity which at 0.1C rate, a reversible capacity of 162 mAhg^{-1} can be achieved. Obviously, the LiFePO_4/C nanofibers prepared using a combination of electrospinning and sol gel methods exhibit superior electrochemical performance compared to currently used cathodes in lithium ion batteries, which can be ascribed to the effect of one-dimensional LiFePO_4 nanostructures with uniformly dispersed carbon on the surface and large

surface-to-volume ratios on the nanofibers.

ACKNOWLEDGMENTS

The authors thank the Ministry of Science and Technology of Taiwan for the financial support for this work under contract no. NSC-101-2113-M-390-004-. We also thank Prof. James R. Carey of the National University of Kaohsiung for grammar correction and helpful discussions.

References

1. S.M. Rezvanizani, Z. Liu, Y. Chen, J. Lee, *J. Power Sources*, 256 (2014) 110-124.
2. J.B. Goodenough, Y. Kim, *Chem. Mater.*, 22 (2010) 587-603.
3. V. Aravindan, J. Gnanaraj, Y.-S. Lee, S. Madhavi, *J. Mater. Chem. A*, 1 (2013) 3518.
4. M. Park, X. Zhang, M. Chung, G.B. Less, A.M. Sastry, *J. Power Sources*, 195 (2010) 7904-7929.
5. M.M. Thackeray, C. Wolverton, E.D. Isaacs, *Energy Environ. Sci.*, 5 (2012) 7854.
6. B.L. Ellis, K.T. Lee, L.F. Nazar, *Chem. Mater.*, 22 (2010) 691-714.
7. P.G. Bruce, B. Scrosati, J.M. Tarascon, *Angew. Chem. Int. Ed.*, 47 (2008) 2930-2946.
8. K.F. Hsu, S.Y. Tsay, B.J. Hwang, *J. Mater. Chem.*, 14 (2004) 2690.
9. M. Li, L. Sun, K. Sun, S. Yu, R. Wang, H. Xie, *J. Solid State Electrochem.*, 16 (2012) 3581-3586.
10. M.S. Whittingham, *Chem. Rev.*, 104 (2004) 4271-4301.
11. M.R. Yang, T.H. Teng, S.H. Wu, *J. Power Sources*, 159 (2006) 307-311.
12. S.C. Jheng, J.S. Chen, *Int. J. Electrochem. Sci.*, 8 (2013) 4901-4913.
13. J.H. Lin, J.S. Chen, *Electrochim. Acta*, 62 (2012) 461-467.
14. W.J. Zhang, *J. Power Sources*, 196 (2011) 2962-2970.
15. Y.-F. Wu, Y.-N. Liu, S.-W. Guo, S.-N. Zhang, T.-N. Lu, Z.-M. Yu, C.-S. Li, Z.-P. Xi, *J. Power Sources*, 256 (2014) 336-344.
16. J. Mun, H.-W. Ha, W. Choi, *J. Power Sources*, 251 (2014) 386-392.
17. F. Croce, A. D'Epifanio, J. Hassoun, A. Deptula, T. Olczac, B. Scrosati, *Electrochem. Solid-State Lett.*, 5 (2002) A47.
18. Y. Wang, G. Cao, *Adv. Mater.*, 20 (2008) 2251-2269.
19. S. Yu, S. Dan, G. Luo, W. Liu, Y. Luo, X. Yu, Y. Fang, *J. Solid State Electrochem.*, 16 (2011) 1675-1681.
20. G. Kucinskis, G. Bajars, J. Kleperis, *J. Power Sources*, 240 (2013) 66-79.
21. D. Lepage, F. Sobh, C. Kuss, G. Liang, S.B. Schougaard, *J. Power Sources*, 256 (2014) 61-65.
22. J.W. Fergus, *J. Power Sources*, 195 (2010) 939-954.
23. C.W. Ong, Y.K. Lin, J.S. Chen, *J. Electrochem. Soc.*, 154 (2007) A527.
24. K.S. Park, J.T. Son, H.T. Chung, S.J. Kim, C.H. Lee, K.T. Kang, H.G. Kim, *Solid State Commun.*, 129 (2004) 311-314.
25. Y.W. Chen, J.S. Chen, *Int. J. Electrochem. Sci.*, 7 (2012) 8128-8139.
26. X. Yin, K. Huang, S. Liu, H. Wang, H. Wang, *J. Power Sources*, 195 (2010) 4308-4312.
27. H.C. Wang, J.R. Carey, J.S. Chen, *Int. J. Electrochem. Sci.*, 5 (2010) 1090-1102.
28. K. Yang, Z. Deng, J. Suo, *J. Solid State Electrochem.*, 16 (2012) 2805-2813.
29. D. Shao, J. Wang, X. Dong, W. Yu, G. Liu, F. Zhang, L. Wang, *J. Mater. Sci. - Mater. Electron.*, 24 (2013) 4263-4269.
30. J.P. Cheng, B.B. Wang, M.G. Zhao, F. Liu, X.B. Zhang, *Sensors and Actuators B: Chemical*, 190 (2014) 78-85.
31. M. Yanilmaz, Y. Lu, M. Dirican, K. Fu, X. Zhang, *Journal of Membrane Science*, 456 (2014) 57-65.
32. J. Miao, M. Miyauchi, J.S. Dordick, R.J. Linhardt, *J. Nanosci. Nanotechnol.*, 12 (2012) 2387-2393.
33. E. Hosono, Y. Wang, N. Kida, M. Enomoto, N. Kojima, M. Okubo, H. Matsuda, Y. Saito, T. Kudo,

- I. Honma, H. Zhou, *ACS Appl Mater Interfaces*, 2 (2010) 212-218.
34. C. Zhu, Y. Yu, L. Gu, K. Weichert, J. Maier, *Angew. Chem. Int. Ed.*, 50 (2011) 6278-6282.
35. O. Toprakci, L. Ji, Z. Lin, H.A.K. Toprakci, X. Zhang, *J. Power Sources*, 196 (2011) 7692-7699.
36. O. Toprakci, H.A. Toprakci, L. Ji, G. Xu, Z. Lin, X. Zhang, *ACS Appl Mater Interfaces*, 4 (2012) 1273-1280.
37. W. Peng, L. Jiao, H. Gao, Z. Qi, Q. Wang, H. Du, Y. Si, Y. Wang, H. Yuan, *J. Power Sources*, 196 (2011) 2841-2847.
38. M.L. Ruiz, I.D. Lick, M.I. Ponzi, E.R. Castellón, A. Jiménez-López, E.N. Ponzi, *Thermochimica Acta*, 499 (2010) 21-26.
39. A.V. Korobeinyk, R.L.D. Whitby, S.V. Mikhalovsky, *Eur. Polym. J.*, 48 (2012) 97-104.
40. S. Franger, F. Le Cras, C. Bourbon, H. Rouault, *J. Power Sources*, 119-121 (2003) 252-257.
41. Y. Xia, M. Yoshio, H. Noguchi, *Electrochim. Acta*, 52 (2006) 240-245.

© 2014 The Authors. Published by ESG (www.electrochemsci.org). This article is an open access article distributed under the terms and conditions of the Creative Commons Attribution license (<http://creativecommons.org/licenses/by/4.0/>).